JCI The Journal of Clinical Investigation

Bronchus-associated lymphoid tissue–resident Foxp3$^+$ T lymphocytes prevent antibody-mediated lung rejection

Wenjun Li, Jason M. Gauthier, Ryuji Higashikubo, Hsi-Min Hsiao, Satona Tanaka, Linh Vuong, Jon H. Ritter, Alice Y. Tong, Brian W. Wong, Ramsey R. Hachem, Varun Puri, Ankit Bharat, Alexander S. Krupnick, Chyi S. Hsieh, William M. Baldwin III, Francine L. Kelly, Scott M. Palmer, Andrew E. Gelman, Daniel Kreisel

J Clin Invest. 2018. https://doi.org/10.1172/JCI122083.

Research Article **Immunology**

Antibody-mediated rejection (AMR) is a principal cause of acute and chronic failure of lung allografts. However, mechanisms mediating this oftentimes fatal complication are poorly understood. Here, we show that Foxp3$^+$ T cells formed aggregates in rejection-free human lung grafts and accumulated within induced bronchus-associated lymphoid tissue (BALT) of tolerant mouse lungs. Using a retransplantation model, we show that selective depletion of graft-resident Foxp3$^+$ T lymphocytes resulted in the generation of donor-specific antibodies (DSA) and AMR, which was associated with complement deposition and destruction of airway epithelium. AMR was dependent on graft infiltration by B and T cells. Depletion of graft-resident Foxp3$^+$ T lymphocytes resulted in prolonged interactions between B and CD4$^+$ T cells within transplanted lungs, which was dependent on CXCR5-CXCL13. Blockade of CXCL13 as well as inhibition of the CD40 ligand and the ICOS ligand suppressed DSA production and prevented AMR. Thus, we have shown that regulatory Foxp3$^+$ T cells residing within BALT of tolerant pulmonary allografts function to suppress B cell activation, a finding that challenges the prevailing view that regulation of humoral responses occurs peripherally. As pulmonary AMR is largely refractory to current immunosuppression, our findings provide a platform for developing therapies that target local immune responses.

Bronchus-associated lymphoid tissue–resident Foxp3+ T lymphocytes prevent antibody-mediated lung rejection

Wenjun Li,[1] Jason M. Gauthier,[1] Ryuji Higashikubo,[1] Hsi-Min Hsiao,[1] Satona Tanaka,[1] Linh Vuong,[1] Jon H. Ritter,[2] Alice Y. Tong,[1] Brian W. Wong,[1] Ramsey R. Hachem,[3] Varun Puri,[1] Ankit Bharat,[4] Alexander S. Krupnick,[5] Chyi S. Hsieh,[3] William M. Baldwin III,[6] Francine L. Kelly,[7] Scott M. Palmer,[7] Andrew E. Gelman,[1,2] and Daniel Kreisel[1,2]

[1]Department of Surgery, [2]Department of Pathology & Immunology, and [3]Department of Medicine, Washington University in St. Louis, St. Louis, Missouri, USA. [4]Department of Surgery, Northwestern University, Chicago, Illinois, USA. [5]Department of Surgery, The University of Virginia, Charlottesville, Virginia, USA. [6]Department of Immunology, Cleveland Clinic, Lerner Research Institute, Cleveland, Ohio, USA. [7]Department of Medicine, Duke University, Durham, North Carolina, USA.

Antibody-mediated rejection (AMR) is a principal cause of acute and chronic failure of lung allografts. However, mechanisms mediating this oftentimes fatal complication are poorly understood. Here, we show that Foxp3+ T cells formed aggregates in rejection-free human lung grafts and accumulated within induced bronchus-associated lymphoid tissue (BALT) of tolerant mouse lungs. Using a retransplantation model, we show that selective depletion of graft-resident Foxp3+ T lymphocytes resulted in the generation of donor-specific antibodies (DSA) and AMR, which was associated with complement deposition and destruction of airway epithelium. AMR was dependent on graft infiltration by B and T cells. Depletion of graft-resident Foxp3+ T lymphocytes resulted in prolonged interactions between B and CD4+ T cells within transplanted lungs, which was dependent on CXCR5-CXCL13. Blockade of CXCL13 as well as inhibition of the CD40 ligand and the ICOS ligand suppressed DSA production and prevented AMR. Thus, we have shown that regulatory Foxp3+ T cells residing within BALT of tolerant pulmonary allografts function to suppress B cell activation, a finding that challenges the prevailing view that regulation of humoral responses occurs peripherally. As pulmonary AMR is largely refractory to current immunosuppression, our findings provide a platform for developing therapies that target local immune responses.

Introduction

Lung transplantation is the only treatment available for numerous patients suffering from end-stage pulmonary failure. Compared with outcomes for other organ transplants, that after lung transplantation remains far worse, with a median survival of approximately 6 years (1). Immunosuppressive strategies for lung transplant patients have been developed largely based on experience with transplant of other organs, such as kidneys and livers. However, we and others have shown that immune responses to lungs are substantially different from those to other transplanted organs, raising concern about the efficacy of treatment algorithms currently used in the clinics (2). Lungs provide a suitable environment for the activation of immune cells, setting pulmonary grafts apart from other transplantable solid organs, where the generation of immune responses depends on trafficking to draining secondary lymphoid organs (3–6). To this end, we have shown that both proinflammatory and regulatory immune pathways can be generated within the lung graft itself (6, 7).

▶ Related Commentary: https://doi.org/10.1172/JCI126517

Conflict of interest: DK has a pending patent entitled "Compositions and methods for detecting CCR2 receptors" (application number 15/611,577). DK also serves on the Scientific Advisory Board of Compass Therapeutics and has received research support from Compass Therapeutics.

Submitted: May 8, 2018; **Accepted:** November 6, 2018.
Reference information: *J Clin Invest*. https://doi.org/10.1172/JCI122083.

We have previously reported that $CD44^{hi}CD62L^{hi}CCR7^{+}CD8^{+}$ central memory T cells are critical for inducing tolerance after lung transplantation (5). Mechanistically, we demonstrated that acute cellular rejection is prevented by graft-infiltrating central memory $CD8^{+}$ T cells through IFN-γ–dependent induction of nitric oxide production. Interestingly, acute cellular rejection in the absence of $CD8^{+}$ T lymphocytes was associated with reduced frequencies of graft-infiltrating $CD4^{+}Foxp3^{+}$ T cells early after transplantation. This raises the possibility that $CD8^{+}$ T cell–mediated induction of tolerance facilitates enrichment of the pulmonary graft with $Foxp3^{+}$ cells. We have also observed that, at later stages, bronchus-associated lymphoid tissue (BALT) is induced in accepted murine lung allografts and enriched in $Foxp3^{+}$ T cells (7). In this study, we used a murine lung retransplant model to determine whether graft-resident $Foxp3^{+}$ T lymphocytes are critical to maintaining a tolerant state. Interestingly, when graft-resident $Foxp3^{+}$ T cells were depleted from long-term tolerant grafts, donor-specific antibodies (DSA) were produced, and surprisingly, grafts underwent antibody-mediated rejection (AMR), a rejection pattern distinct from the acute cellular rejection previously observed when $CD8^{+}$ T cells were absent during tolerance induction. AMR following depletion of $Foxp3^{+}$ cells depended on graft infiltration by B and T cells and could be prevented by inhibiting pathways that mediate interactions between T follicular helper (Tfh) cells and B lymphocytes. As AMR of transplanted lungs is generally refractory to currently employed treatment, often resulting in graft failure and patient death, our findings provide a mechanistic framework for the development of new therapeutic strategies for this clinically vexing problem.

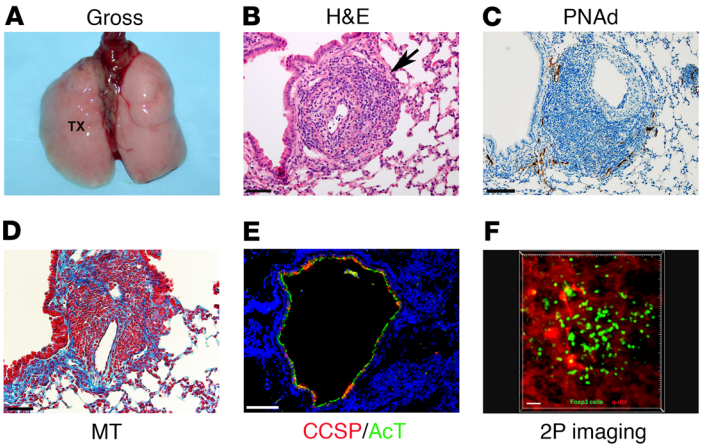

Figure 1. Long-term acceptance after lung transplantation is associated with induction of Foxp3⁺ cell–rich BALT. (**A**) Gross and (**B**) histological appearance (H&E) of BALB/c lung graft (Tx) at least 30 days after transplantation into an immunosuppressed B6 host. Arrow depicts induced BALT (n = 8). Scale bar: 100 μm. (**C**) PNAd staining (brown), (**D**) MT staining (blue), and (**E**) immunofluorescent staining of CCSP (red) and AcT (green) in BALB/c lung graft at least 30 days after transplantation into an immunosuppressed B6 host. Scale bars: 100 μm. (**F**) Intravital 2-photon (2P) imaging depicting aggregates of Foxp3⁺ cells in BALB/c lung graft at least 30 days after transplantation into an immunosuppressed B6 Foxp3-IRES GFP recipient (Foxp3⁺ cells, green; quantum dot–labeled vessels, red) (n = 3). Scale bar: 30 μm.

Results

Tolerance induction after lung transplantation is associated with induction of Foxp3⁺ T cell–rich BALT and normal airway epithelium. Immunosuppression-mediated long-term acceptance of transplanted lungs is associated with the induction of BALT (Figure 1, A and B, and Supplemental Figure 1A; supplemental material available online with this article; https://doi.org/10.1172/JCI122083DS1). Histologically normal airway architecture is noted with thin epithelium (Figure 1B) resembling the appearance of airway epithelium in human lung grafts that have no histological evidence of rejection (Supplemental Figure 2A). Peripheral nodal addressin (PNAd), a hallmark of high endothelial venules, was expressed within the BALT of accepted lungs (Figure 1C). In contrast, PNAd was not expressed in perivascular infiltrates in lung grafts during acute cellular rejection (Supplemental Figure 1, B and C). Only minimal perivascular or peribronchiolar collagen was detected by Masson's trichrome (MT) staining in the murine grafts (Figure 1D). The epithelium was shown to be predominantly ciliated airway epithelial cells expressing apical acetylated tubulin (AcT), a marker of ciliated cells, and occasional club cells expressing club cell secretory protein (CCSP) (Figure 1E). To further characterize the Foxp3⁺ cells, we transplanted BALB/c lungs into C57BL/6 (B6) Foxp3-GFP recipients that were treated with perioperative costimulatory blockade and imaged the grafts by intravital 2-photon microscopy at least 30 days after engraftment. We visualized aggregates of Foxp3⁺ cells within the lung allografts, which displayed little motility (Figure 1F, Supplemental Video 1). We also observed lymphoid aggregates that were enriched in Foxp3⁺ cells in human pulmonary transplant recipients that had no histological evidence of graft rejection at least 6 months after lung engraftment (Supplemental Figure 2B).

To assess whether systemic tolerance is induced after lung transplantation, we transplanted BALB/c hearts into B6 mice that had received BALB/c lungs at least 30 days prior to cardiac engraftment. While BALB/c hearts were acutely rejected after transplantation into naive nonimmunosuppressed B6 mice, they survived indefinitely in B6 hosts that had accepted BALB/c lung grafts (Supplemental Figure 3, A–C). These BALB/c hearts showed no evidence of chronic rejection upon histological examination (Supplemental Figure 3B). When we transplanted third-party CBA hearts into B6 mice that had previously received BALB/c lungs, we observed prolonged survival compared with that in CBA cardiac grafts that were transplanted into naive nonimmunosuppressed B6 mice (Supplemental Figure 3, D–F). However, all CBA hearts that were transplanted into previous BALB/c lung allograft recipients were eventually rejected and displayed histological hallmarks of acute and chronic rejection (Supplemental Figure 3E).

Depletion of graft-resident Foxp3⁺ T cells triggers AMR. We have previously reported that long-term accepted lung grafts are not rejected after retransplantation into nonimmunosuppressed allogeneic hosts, indicating that immunoregulatory pathways are established in tolerant pulmonary grafts that protect them from immunological destruction (7). To determine whether graft-resident Foxp3⁺ T lymphocytes contribute to maintenance of lung tolerance, we took advantage of our recently described technique for lung retransplantation (7). To this end, we transplanted BALB/c lungs into B6 CD45.2 WT or B6 CD45.2 Foxp3–diphtheria toxin receptor (Foxp3-DTR) recipients that were treated with perioperative costimulatory blockade. At least 30 days after engraftment, a time point when virtually all graft-resident T cells are derived from the recipient (Supplemental Figure 4), these lungs were retransplanted into nonimmunosuppressed B6 CD45.1 secondary hosts that were treated with diphtheria toxin (DT). Unlike DT treatment of primary Foxp3-DTR lung recipients, which resulted in global elimination of Foxp3⁺ cells (Supplemental Figure 5), this approach allowed us to selectively deplete Foxp3⁺ T cells that resided in the tolerant BALB/c lung graft at the time of retransplantation without targeting cells in the secondary recipient (Figure 2, A–C). Approximately one-third of Foxp3⁺ cells that were present in control retransplanted grafts had originated from the primary recipient, while virtually all Foxp3⁺ cells were derived from the secondary host when graft-resident Foxp3⁺ cells were depleted at the time of retransplantation (Figure 2D). The majority of Foxp3⁺ cells in retransplanted tolerant lungs that were derived from the primary donor expressed CD4, while only a small portion expressed CD8 (Supplemental Figure 6). Also, the proportion of Foxp3⁺ cells in retransplanted grafts that originated from the primary host was higher when lungs were retransplanted 30 days compared with 72 hours after the initial transplantation (Supplemental Figure 7 and Figure 2D). At 7 days after retransplantation, control grafts were ventilated, showed mild inflammation, and retained BALT containing B and T lymphocytes as well as PNAd⁺ cells, while, in

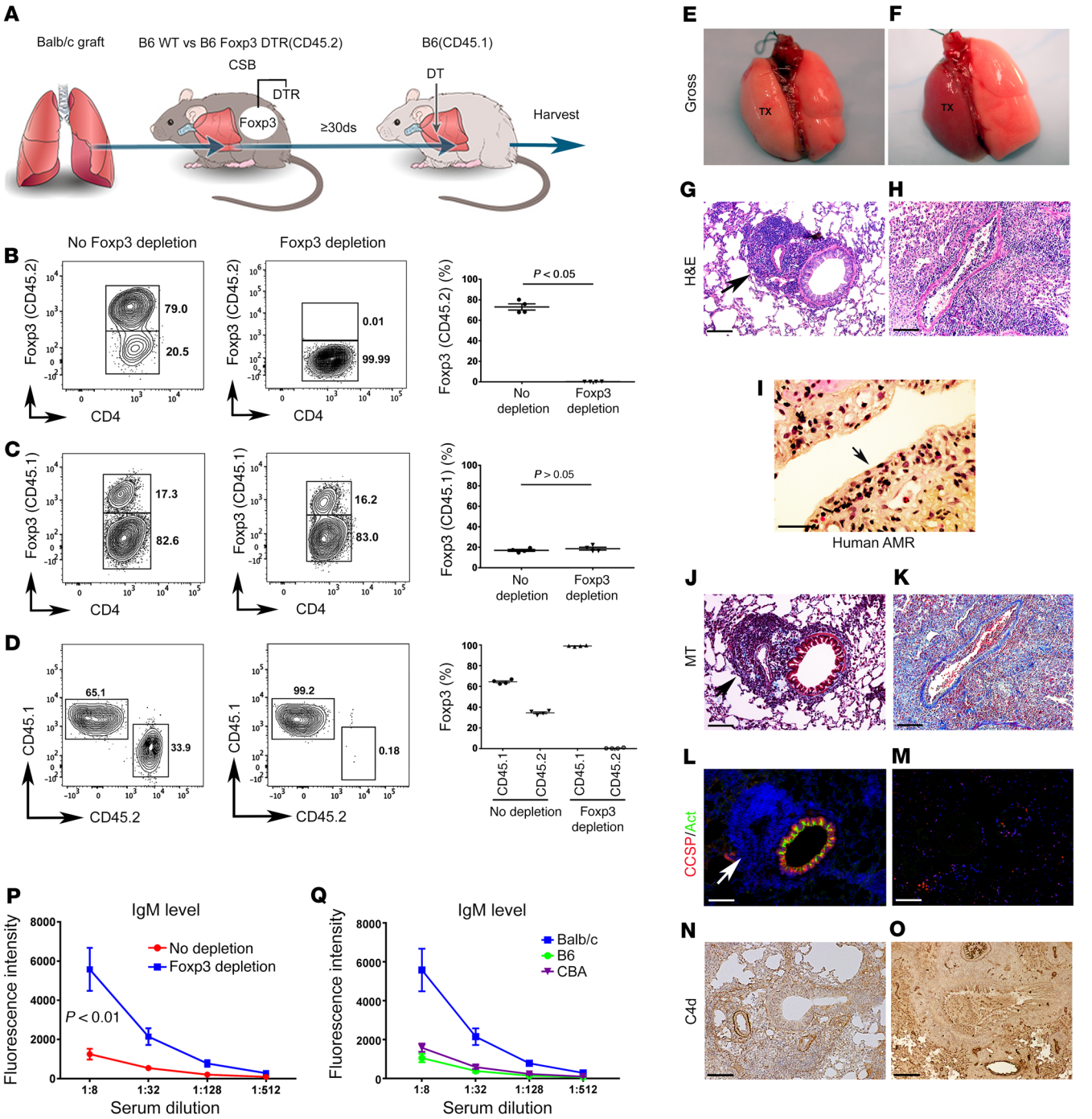

Figure 2. Depletion of graft-resident Foxp3⁺ T cells triggers AMR. (**A**) Schematic depicting experimental model. CSB, costimulation blockade. Plots and quantification of CD4⁺Foxp3⁺ cells from (**B**) primary (CD45.2) or (**C**) secondary recipient (CD45.1) in BALB/c lungs, transplanted into immunosuppressed WT B6 (CD45.2) (circles) or Foxp3-DTR B6 (CD45.2) (inverted triangles) mice and retransplanted into DT-treated B6 (CD45.1) hosts at least 30 days later. Plots are gated on live CD45.2⁺CD45.1⁻CD90.2⁺ and live CD45.2⁻CD45.1⁺CD90.2⁺ cells. (**D**) Plots and quantification of distribution of CD45.1 vs. CD45.2 on live CD90.2⁺CD4⁺CD8⁻Foxp3⁺ cells without and with depletion of graft-resident (CD45.2) Foxp3⁺ cells. Gross and histological appearance (H&E) of BALB/c lungs, transplanted into immunosuppressed WT (**E** and **G**) or Foxp3-DTR (**F** and **H**) B6 CD45.2⁺ mice and, at least 30 days later, retransplanted into DT-treated B6 CD45.1⁺ hosts (n = 4 mice per group). (**I**) Airway epithelium (arrow) in human lung diagnosed with AMR (H&E) (n = 11). Staining of (**J** and **K**) MT (blue), (**L** and **M**) CCSP (red), AcT (green), and (**N** and **O**) C4d (brown) in BALB/c lungs, transplanted into immunosuppressed (**J**, **L**, and **N**) WT or (**K**, **M**, and **O**) Foxp3-DTR B6 CD45.2⁺ mice and, at least 30 days later, retransplanted into DT-treated B6 CD45.1⁺ hosts. Scale bars: 100 μm. Arrows in **G**, **J**, and **L** point to BALT. (**P**) Donor-specific IgM antibody titers 7 days after retransplantation of BALB/c lungs into DT-treated B6 CD45.1⁺ hosts at least 30 days after initial engraftment into immunosuppressed B6 WT (red) or B6 Foxp3-DTR (blue) mice. (**Q**) Reactivity of serum IgM antibodies, following depletion of graft-resident Foxp3 cells, against donor (BALB/c), recipient (B6), and third-party (CBA) antigen (n = 4 mice per group). Data are expressed as mean ± SEM. Mann-Whitney U test was used to compare the means.

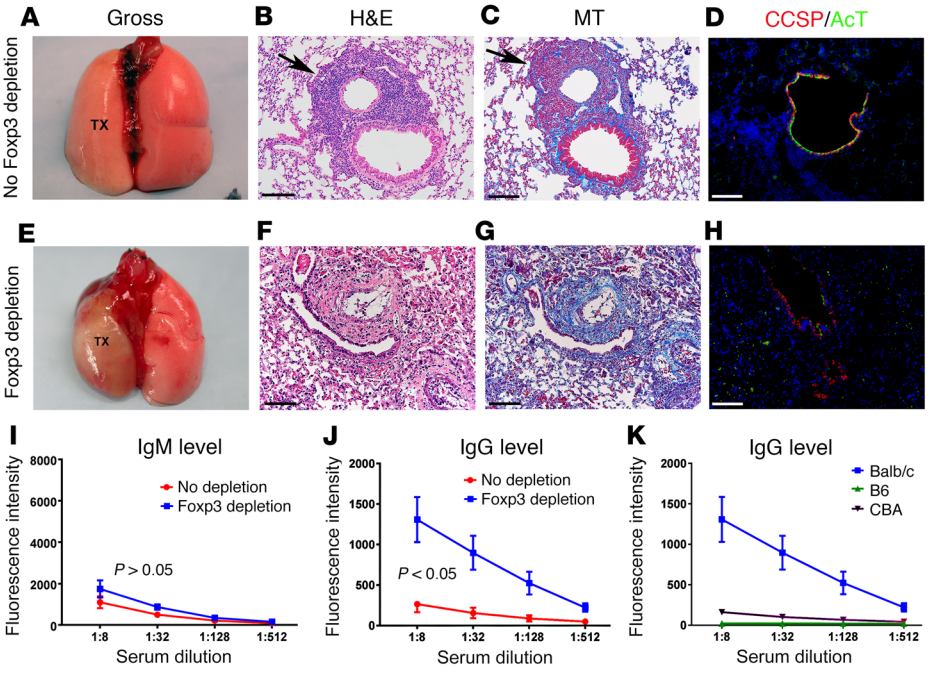

Figure 3. Graft-resident Foxp3⁺ T cells maintain lung transplant tolerance. (**A** and **E**) Gross and (**B** and **F**) histological appearance (H&E), (**C** and **G**) MT staining (blue), and (**D** and **H**) immunofluorescent staining of CCSP (red) and AcT (green) in BALB/c lungs, initially transplanted into immunosuppressed (**A**–**D**) B6 (CD45.2⁺) or (**E**–**H**) B6 Foxp3-DTR (CD45.2⁺) mice and retransplanted into DT-treated secondary B6 (CD45.1⁺) hosts at least 30 days after primary transplantation. Secondary hosts were examined 30 days after retransplantation. Scale bars: 100 μm. Arrows in **B** and **C** point to BALT. Serum titers of donor-specific (**I**) IgM and (**J**) IgG antibodies 30 days after retransplantation of BALB/c lungs, initially transplanted into immunosuppressed B6 WT (red) or B6 Foxp3-DTR (blue) mice and, at least 30 days later, retransplanted into B6 45.1⁺ hosts. (**K**) Reactivity of serum IgG antibodies, following depletion of graft-resident Foxp3 cells, against donor (BALB/c), recipient (B6), and third-party (CBA) antigen. Data are expressed as mean ± SEM (n = 4 mice per group). Mann-Whitney U test was used to compare the means.

contrast, Foxp3⁺ T cell depletion resulted in severe inflammation with histological evidence of hyaline membrane formation, alveolar edema, fibrinous deposits within the alveoli, and arteriolar fibrinoid necrosis, hallmarks of AMR in human lung grafts (Figure 2, E–H) (Supplemental Figure 8). Notably, these grafts showed no histological evidence of cellular rejection. Retransplantation of BALB/c lungs that were initially transplanted into B6 CD45.2 Foxp3-DTR hosts and, at least 30 days later, retransplanted into PBS-treated secondary recipients yielded results comparable to those seen in retransplantation of BALB/c grafts that were initially transplanted into B6 CD45.2 WT hosts and then retransplanted into DT-treated secondary B6 CD45.1 mice (data not shown). Of note, most Foxp3⁺ T lymphocytes that had infiltrated the allograft from the primary recipient expressed CD25 and intracellular CTLA4 and displayed an effector memory phenotype ($CD44^{hi}$ $CD62L^{lo}$). Moreover, the majority of Foxp3⁺ T cells expressed the proliferation marker Ki-67, and a small percentage of the Foxp3⁺ T lymphocytes expressed markers characteristic of T follicular regulatory (Tfr) cells (Supplemental Figure 9). When we evaluated the airway epithelium in the Foxp3⁺ T cell–depleted tissue, the epithelium was completely destroyed, with epithelial remnants in the airway lumen (Figure 2H), in contrast with the control airway with hyperplastic epithelium (Figure 2G). The airway changes in the Foxp3⁺ T lymphocyte–depleted murine grafts were reminiscent of those observed in human pulmonary grafts that underwent AMR (Figure 2I). We also observed abnormal parenchyma with interstitial fibrosis following depletion of graft-resident Foxp3⁺ T cells (Figure 2, J and K). Furthermore, in contrast to control retransplanted lungs, characterization of the airway epithelium by immunofluorescence of CCSP and AcT confirmed the absence of these normal epithelial markers in Foxp3⁺ T lymphocyte–depleted grafts, while the denuded intraluminal epithelial remnant stained for CCSP (Figure 2, L and M). We also observed deposition of complement fragments on endothelial cells in arterioles, venules, and capillaries, and serum titers of donor-specific IgM antibodies were significantly elevated following depletion of Foxp3⁺ T cells (Figure 2, N–P). Reactivity of the serum IgM antibodies against donor antigen was significantly higher than against recipient or third-party antigen (Figure 2Q).

At 30 days after retransplantation, control grafts displayed preserved lung architecture with induced BALT (Figure 3, A and B). In contrast, by gross examination, Foxp3⁺ T lymphocyte–depleted grafts appeared necrotic at 30 days after retransplantation (Figure 3E). Interestingly, the airway epithelium 30 days after Foxp3⁺ T cell depletion showed some regeneration and hyperproliferation (Figure 3F). The parenchyma continued to appear abnormal, with increased fibrosis as well as substantial peribronchiolar and perivascular collagen deposition, while in comparison, control grafts showed minimal MT staining (Figure 3, C and G). Although the epithelium had regenerated and abundant AcT was detected, the expression of CCSP was aberrant, as it was absent throughout most of the airway, but present in confined areas, compared with the normal distribution seen in the control grafts (Figure 3, D and H). Interestingly, this is consistent with previous reports in humans showing an association between decreased CCSP expression and chronic rejection after lung transplantation (8). In addition to airway epithelial changes, we detected disorganized endothelium in the Foxp3⁺ T cell–depleted pulmonary grafts, where it appeared necrotic in some areas and the vessel lumen was filled with debris (Figure 3F). Serum levels of donor-specific IgG, but not IgM, were significantly higher 30 days after depletion of Foxp3⁺ T lymphocytes (Figure 3, I and J). Similarly to our observations for IgM antibodies on day 7, reactivity of the serum IgG antibodies against donor antigen was significantly higher than against recipient or third-party antigen (Figure 3K).

Foxp3⁺ T cell depletion–triggered AMR is dependent on graft-infiltrating B cells. Having shown that transplanted lungs have histological changes consistent with AMR after depletion of graft-

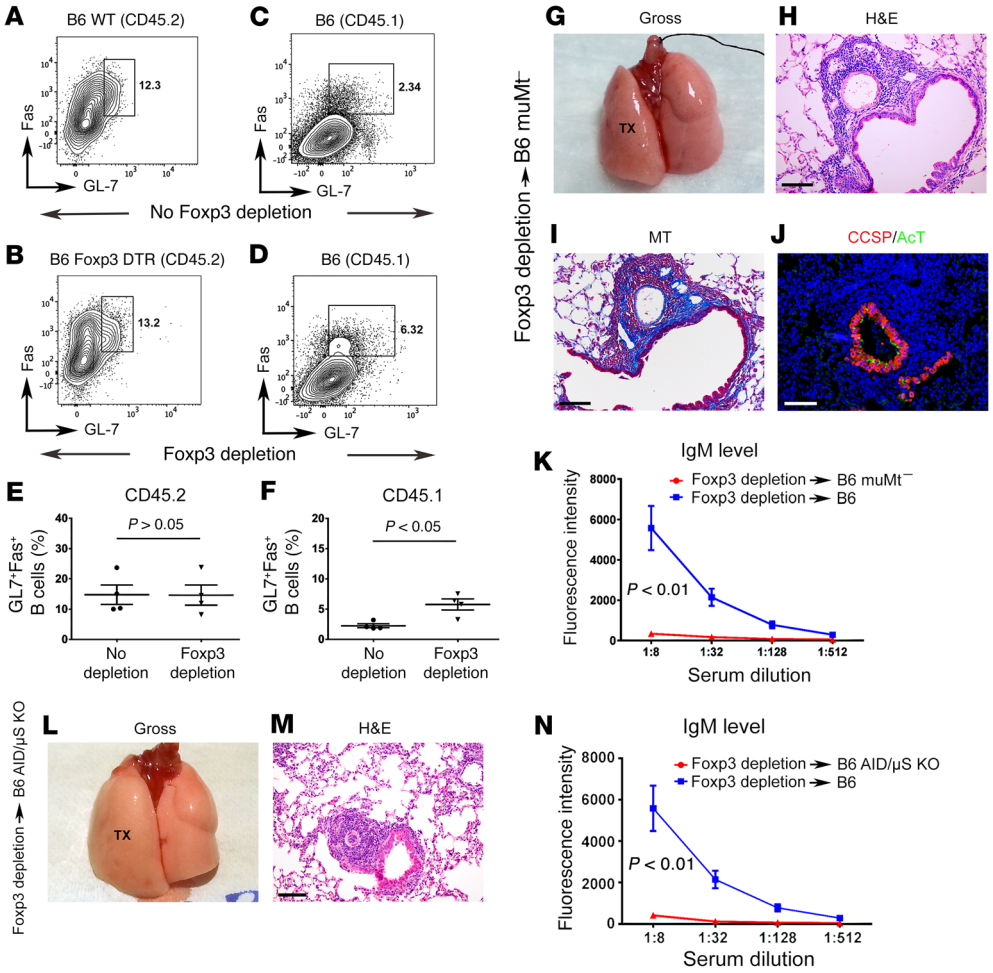

Figure 4. Graft-infiltrating B cells trigger AMR after depletion of graft-resident Foxp3⁺ T cells. Activated B cells from (**A** and **B**) primary recipient (CD45.2) or (**C** and **D**) secondary recipient (CD45.1) in BALB/c lungs, transplanted into immunosuppressed (**A** and **C**) B6 (CD45.2⁺) (no Foxp3 depletion) or (**B** and **D**) B6 Foxp3-DTR (CD45.2⁺) mice (Foxp3 depletion) and, at least 30 days later, retransplanted into DT-treated B6 (CD45.1⁺) hosts. Plots are gated on live CD45.2⁺CD45.1⁻B220⁺ (donor) and live CD45.2⁻CD45.1⁺B220⁺ cells (recipient). Quantification of activated (**E**) CD45.2 and (**F**) CD45.1 B cells in (circles) control and (inverted triangles) Foxp3⁺ T cell–depleted lungs 7 days after retransplantation. (**G**) Gross, (**H**) histological appearance (H&E), (**I**) MT staining (blue), and (**J**) CCSP (red) and AcT (green) staining in BALB/c lungs, transplanted into immunosuppressed B6 Foxp3-DTR mice and, at least 30 days later, retransplanted into DT-treated B6 muMt⁻ hosts. (**K**) Donor-specific IgM titers 7 days after retransplantation of BALB/c lungs into DT-treated WT (blue) or muMt⁻ (red) B6 hosts at least 30 days after engraftment into immunosuppressed B6 Foxp3-DTR mice. (**L**) Gross and (**M**) histological appearance (H&E) of BALB/c lungs, transplanted into immunosuppressed B6 Foxp3-DTR mice and, at least 30 days later, retransplanted into DT-treated B6 AID/μS knockout hosts. Scale bars: 100 μm. (**N**) Donor-specific IgM titers 7 days after retransplantation of BALB/c lungs into DT-treated WT (blue) or AID/μS knockout (red) B6 hosts at least 30 days after engraftment into immunosuppressed B6 Foxp3-DTR mice. Data are expressed as mean ± SEM (n = 4 mice per group). Mann-Whitney U test was used to compare the means.

resident Foxp3⁺ T lymphocytes, we next analyzed B lymphocytes in the lung allografts 7 days after retransplantation. The use of congenic CD45.1 secondary recipients allowed us to differentiate between cells that had originated from the primary versus the secondary recipients. We observed a higher percentage of activated B cells from secondary, but not primary, recipient in Foxp3⁺ T cell–depleted grafts (Figure 4, A–F). A very small proportion of B cells in spleens of naive untransplanted mice expressed activation markers (Supplemental Figure 10). To evaluate the role of graft-infiltrating B cells in mediating rejection, we next retransplanted tolerant BALB/c lungs into B6 muMT mice, which lack mature B cells, and depleted the graft-resident Foxp3⁺ T cells at the time of retransplantation. Foxp3⁺ T lymphocyte–depleted grafts were ventilated and showed no evidence of rejection 7 days after retransplantation into B6 muMT mice (Figure 4, G and H). Similarly to tolerant lungs that were retransplanted into WT hosts without depletion of graft-resident Foxp3⁺ cells, these grafts showed evidence of BALT, with B and T lymphocytes as well as PNAd⁺ cells (Supplemental Figure 11, A and B). Preventing B lymphocyte graft infiltration after depletion of Foxp3⁺ T cells resulted in decreased collagen deposition (Figure 4I) compared with our observations in Foxp3⁺ T lymphocyte–depleted pulmonary grafts that were retransplanted into WT hosts (Figure 2K). The epithelial architecture remained intact and appeared hyperproliferative compared with that shown with control grafts (Figure 4H). In addition, we observed an increase in the expression of CCSP and a decrease in the expression of AcT compared with Foxp3⁺ T cell–replete lung grafts, possibly indicating some epithelial repair (Figure 4J). Furthermore, we did not detect donor-specific IgM or IgG antibodies in the serum when secondary recipients lacked mature B cells (Figure 4K) (Supplemental Figure 12).

In addition to their capacity to produce antibodies, B cells have been shown to contribute to graft rejection through antigen presentation (9). As B cells derived from the primary and secondary recipient were present in rejecting grafts, we wanted to determine whether antibody production by B cells that infiltrate the graft from the secondary recipient are critical for mediating graft rejection after Foxp3⁺ T lymphocyte depletion. For this purpose, we depleted Foxp3⁺ T cells from tolerant grafts following retransplantation into activation-induced cytidine deaminase / secretory μ-chain double-knockout mice (B6 AID/μS KO). These mice have B cells that cannot undergo affinity maturation or secrete antibodies of any isotype (9). Similarly to our observations with B cell-deficient secondary recipients,

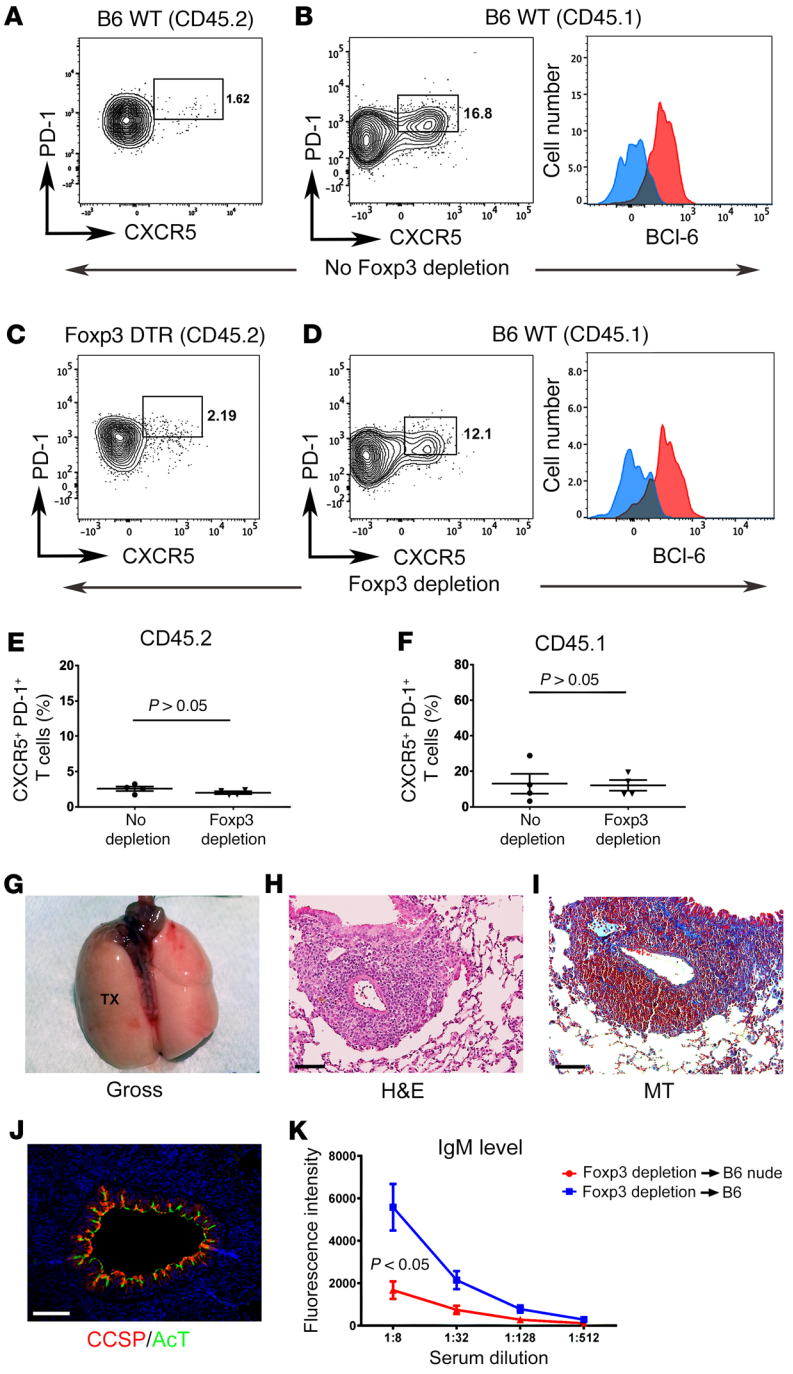

Figure 5. AMR after depletion of graft-resident Foxp3⁺ T cells is dependent on graft infiltration by T cells. Plots and histograms depicting markers characteristic of Tfh cells on CD4⁺ T cells derived from (**A** and **C**) primary (CD45.2) or (**B** and **D**) secondary (CD45.1) recipients in BALB/c lungs, initially transplanted into immunosuppressed (**A** and **B**) B6 (CD45.2⁺) or (**C** and **D**) B6 Foxp3-DTR (CD45.2⁺) mice and, at least 30 days later, retransplanted into DT-treated B6 (CD45.1⁺) hosts. Plots are gated on live CD45.2⁺CD45.1⁻ CD90.2⁺CD4⁺CD8⁻Foxp3⁻ and CD45.2⁺CD45.1⁺CD90.2⁺ CD4⁺CD8⁻Foxp3⁻ cells. Histograms are gated on CD4⁺ T cells that are PD-1^{hi}CXCR5⁺ (bcl-6, red; isotype control, blue) (n = 4 each). Quantification of (**E**) CD45.2⁺ and (**F**) CD45.1⁺ CD4⁺ T cells that are PD-1^{hi}CXCR5⁺ in (circles) control and (inverted triangles) Foxp3⁺ T cell–depleted lungs 7 days after retransplantation. (**G**) Gross and (**H**) histological appearance (H&E) and staining for (**I**) MT, (**J**) CCSP (red), and AcT (green) in BALB/c lungs, transplanted into immunosuppressed B6 Foxp3-DTR mice and, at least 30 days later, retransplanted into DT-treated B6 nude hosts. Scale bars: 100 μm. (**K**) Donor-specific IgM titers 7 days after retransplantation of BALB/c lungs into DT-treated WT (blue) or nude (red) B6 hosts at least 30 days after initial engraftment into immunosuppressed B6 Foxp3-DTR mice. Data are expressed as mean ± SEM (n = 4 mice per group). Mann-Whitney U test was used to compare the means.

secondary recipients lacking the capacity to secrete antibodies did not reject grafts, the grafts retained BALT, and no significant elevations in serum DSA were detected (Figure 4, L–N) (Supplemental Figure 11, C and D). Thus, graft rejection after depletion of Foxp3⁺ T lymphocytes from tolerant pulmonary grafts depends on antibody production by graft-infiltrating B cells.

Foxp3⁺ T cell depletion–triggered AMR is dependent on graft-infiltrating T cells. Antibody production by B cells requires help, which can be provided by Tfh cells, a subset of T lymphocytes. Hallmarks of Tfh cells include expression of CXCR5 and PD-1 as well as the transcription factor Bcl-6. Under both control and Foxp3⁺ T cell–depleted conditions, a fraction of CD4⁺ T cells that had originated from either the primary or secondary recipient expressed phenotypic markers characteristic of Tfh cells (Figure 5, A–F). Only a small percentage of graft-infiltrating CD8⁺ T lymphocytes expressed granzyme B or perforin, irrespective of Foxp3⁺ T cell depletion (Supplemental Figure 13). To determine whether infiltration of T cells from the secondary recipient was necessary for triggering graft rejection following depletion of Foxp3⁺ T lymphocytes, we transplanted BALB/c lungs into B6 Foxp3-DTR mice that were treated with perioperative costimulatory blockade. At least 30 days later, these BALB/c lung grafts were retransplanted into B6 nude secondary recipients that were treated with DT at the time of retransplantation. Seven days after retransplantation,

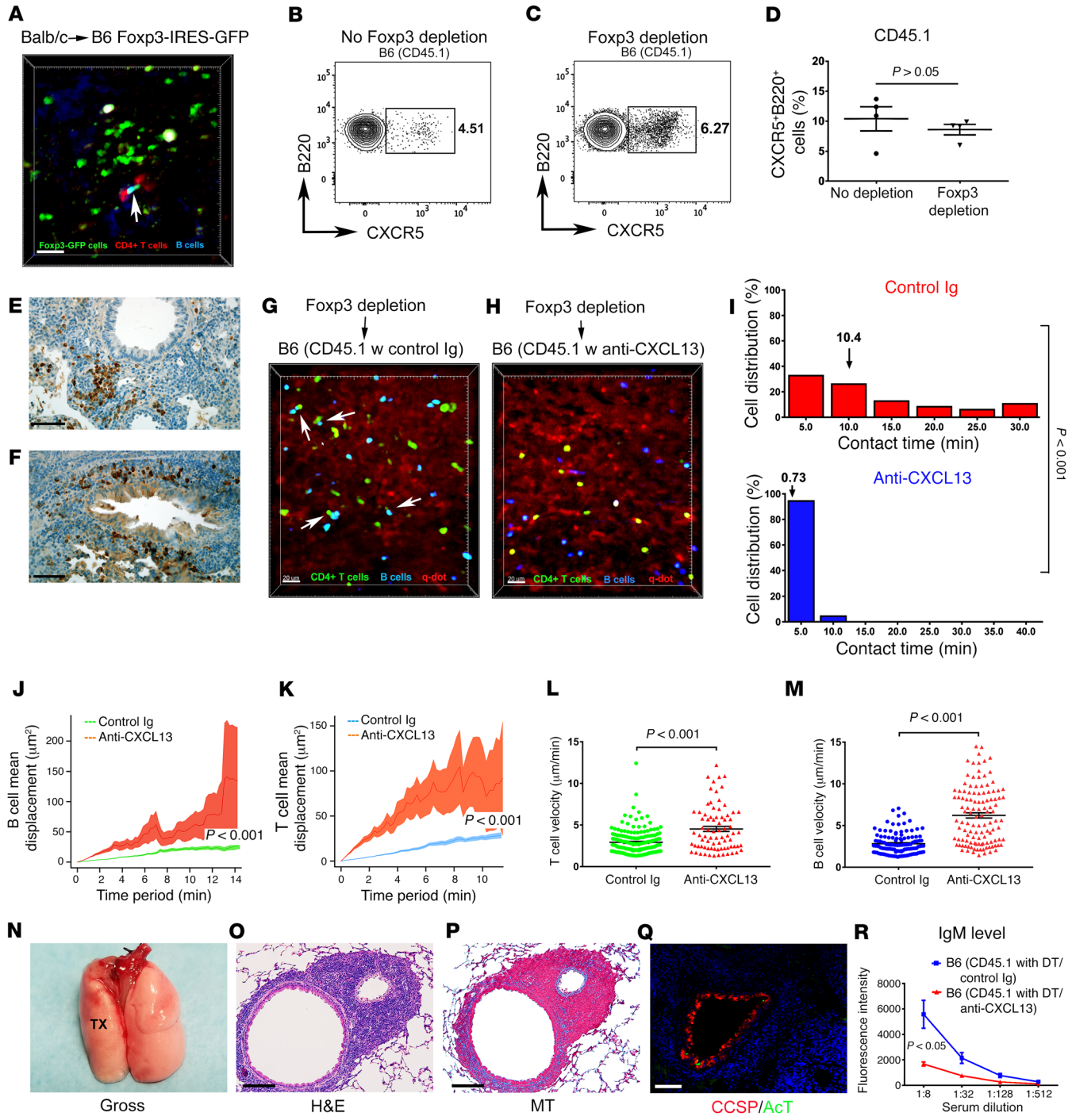

Figure 6. Foxp3⁺ T lymphocyte depletion–triggered AMR is dependent on CXCL13-mediated chemokinesis. (**A**) Foxp3⁺ (green), B cells (blue), and CD4⁺ T cells (red) in BALB/c lungs at least 30 days after transplantation into immunosuppressed B6 Foxp3-IRES GFP recipient (n = 3). Scale bar: 10 μm. CXCR5⁺ B cells from secondary host (recipient) in BALB/c lungs, initially transplanted into immunosuppressed (**B**) WT or (**C**) Foxp3-DTR B6 (CD45.2⁺) recipient and, at least 30 days later, retransplanted into DT-treated B6 CD45.1⁺ hosts. Plots are gated on live CD45.2⁻CD45.1⁺ cells. (**D**) CD45.1⁺CXCR5⁺ B cells in (circles) control and (inverted triangles) Foxp3⁺ T cell–depleted lungs 7 days after retransplantation (n = 4 each). CXCL13 (brown) in (**E**) control and (**F**) Foxp3⁺ T cell–depleted grafts 7 days after retransplantation. Scale bars: 100 μm. CD4⁺ T cells (green) and B cells (blue) in BALB/c lungs, initially transplanted into immunosuppressed B6 Foxp3-DTR recipients and, at least 30 days later, retransplanted into B6 hosts, treated with (**G**) DT/control-Ig (arrows: CD4⁺ T–B cell interactions) or (**H**) DT/anti-CXCL13 (n = 2 each) (red, quantum dots). Scale bars: 20 μm. (**I**) Contact duration between CD4⁺ T and B cells, (**J**) CD4⁺ T, and (**K**) B cell mean square displacements and (**L**) CD4⁺ T and (**M**) B cell velocities within retransplanted Foxp3⁺ T cell–depleted BALB/c lungs with and without CXCL13 inhibition. (**N**) Gross, (**O**) histological appearance (H&E), staining for (**P**) MT (blue), (**Q**) CCSP (red), and AcT (green) in BALB/c lungs, transplanted into immunosuppressed B6 Foxp3-DTR mice and, at least 30 days later, retransplanted into DT- and anti-CXCL13–treated B6 hosts. Scale bars: 100 μm. (**R**) Donor-specific IgM titers after retransplantation of BALB/c lungs into DT-treated control (blue) or DT/anti-CXCL13 antibody–treated (red) B6 recipients after initial engraftment into immunosuppressed B6 Foxp3-DTR mice (n = 4 mice per group). Data are expressed as mean ± SEM. Mann-Whitney U test was used to compare the means.

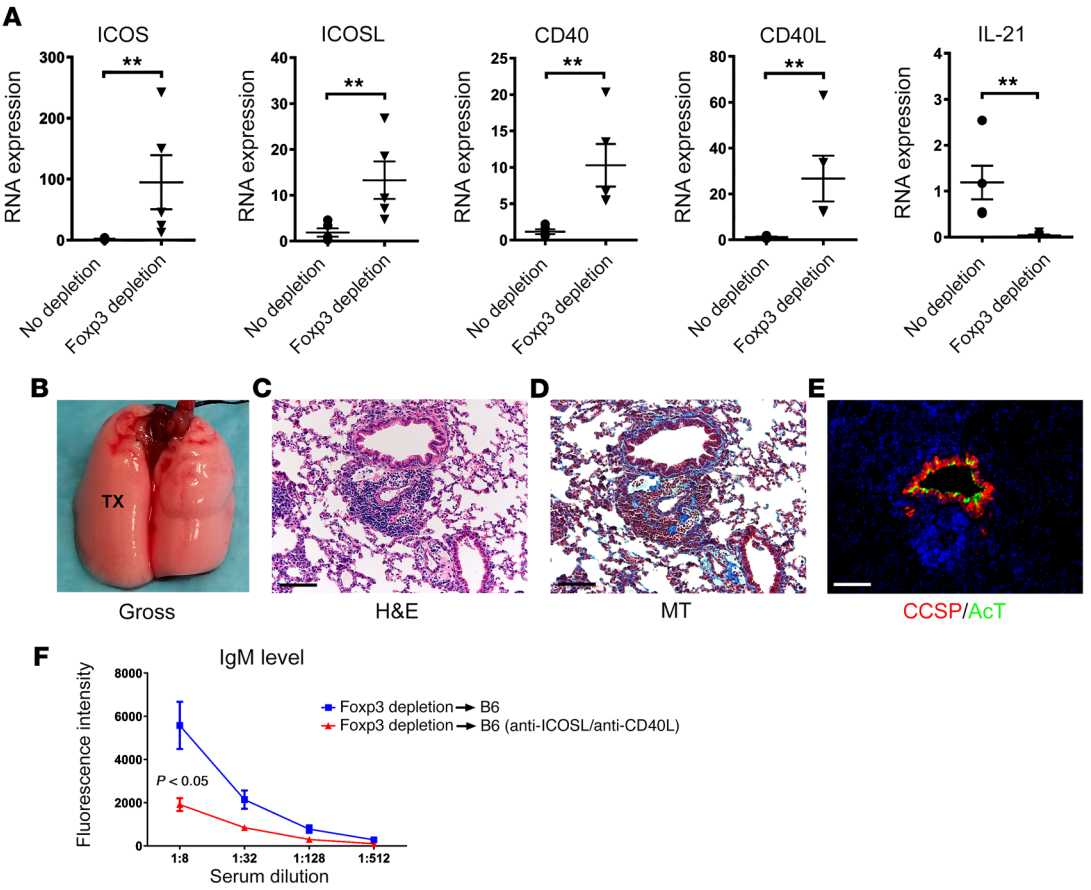

Figure 7. AMR of Foxp3⁺ T cell–depleted lung grafts can be prevented by blocking ICOS/ICOS ligand and CD40/CD40 ligand pathways. (**A**) Expression levels of ICOS, ICOS ligand (ICOSL), CD40, CD40 ligand (CD40L), and IL-21 in BALB/c lung grafts, which were initially transplanted into immunosuppressed B6 WT (CD45.2) (circles) or Foxp3-DTR B6 (CD45.2) (inverted triangles) mice and at least 30 days later retransplanted into DT-treated (days 0 and 1) B6 CD45.1 hosts. Grafts were examined 7 days after retransplantation (n = 5 each). $^{**}P < 0.01$. (**B**) Gross appearance, (**C**) histological appearance (H&E), (**D**) MT (blue) staining, (**E**) and immunofluorescent staining of CCSP (red) and AcT (green) after depletion of graft-resident Foxp3⁺ T cells and 7 days after retransplantation into anti-ICOS ligand and anti-CD40 ligand–treated secondary hosts. Scale bars: 100 μm. (**F**) Serum titers of donor-specific IgM 7 days after retransplantation of BALB/c lungs, initially transplanted into immunosuppressed B6 Foxp3-DTR mice and at least 30 days later retransplanted into DT-treated WT B6 hosts that were treated with anti-ICOS ligand and anti-CD40 ligand (red) or did not receive treatment (blue) (n = 4 mice per group). Data are expressed as mean ± SEM. Mann-Whitney U test was used to compare the means.

these grafts were ventilated and showed no evidence of rejection (Figure 5, G and H). Compared with Foxp3⁺ T cell–replete pulmonary grafts, we observed a slight increase in collagen deposition, and airway epithelium was hyperproliferative (Figure 5, H and I). The expression patterns of CCSP and AcT appeared normal (Figure 5J) and were comparable to those in control Foxp3⁺ T cell–replete lungs (Figure 2L). Serum titers of donor-specific IgM antibodies were low and comparable to those under control conditions, where tolerant BALB/c lungs were retransplanted into secondary B6 hosts without depletion of Foxp3⁺ T lymphocytes (Figure 5K and Figure 2P).

Foxp3⁺ T cell depletion–triggered AMR is dependent on CXCL13-mediated chemokinesis. Having shown that graft-infiltrating T and B cells are both critical in mediating production of DSA and graft rejection after depletion of Foxp3⁺ T cells, we set out to examine cellular interactions within the transplanted lungs. We first evaluated whether graft-resident Foxp3⁺ T lymphocytes interact with B and T cells that infiltrate tolerant lung allografts. For this purpose, we transplanted BALB/c lungs into B6 Foxp3-GFP mice that received perioperative costimulatory blockade. At least 30 days after engraftment of the lungs, we injected recipient-matched CD4⁺ T cells and B cells that were labeled with fluorescent dyes. CD4⁺ T and B cells preferentially migrated to areas in the graft where Foxp3⁺ T cell aggregates were present (Figure 6A and Supplemental Video 2). Both CD4⁺ T and B cells formed prolonged interactions with Foxp3⁺ T cells. As both CXCR5-expressing T and B cells of recipient origin (Figure 5D and Figure 6, B–D) were present in rejecting lung allografts following depletion of Foxp3⁺ T lymphocytes, we next wanted to investigate the role of the CXCR5 ligand CXCL13 in mediating interactions between T and B lymphocytes within lung grafts and promoting rejection. We first determined that CXCL13 was expressed within induced BALT in control tolerant retransplanted lungs and also in the interstitium of lungs that were acutely rejected after depletion of Foxp3⁺ T cells (Figure 6, E and F). We then evaluated how CXCR5-CXCL13 signaling regulates the dynamic behavior of T and B cells that infiltrate Foxp3⁺ T cell–depleted lung allografts. After injection of control antibodies, many T and B cells interacted with each other, often forming durable contacts (Figure 6G, Supplemental Video 3). In contrast, when we

injected CXCL13-neutralizing antibodies, we observed a decrease in the duration of interactions between T and B cells as well as significant increases in their displacements and velocities (Figure 6, H–M, and Supplemental Video 4). Finally, neutralization of CXCL13 concurrent with depletion of Foxp3$^+$ T cells prevented graft rejection and preserved the airway epithelium (Figure 6, N and O). Similarly to our observations after retransplantation of Foxp3$^+$ T lymphocyte–depleted grafts into B cell–deficient hosts, there was some mild degree of peribronchiolar fibrosis, and CCSP expression appeared elevated, while AcT expression was decreased (Figure 6, P and Q). Finally, neutralization of CXCL13 did not result in significant elevation in serum titers of DSA following depletion of Foxp3$^+$ T cells (Figure 6R).

Blockade of CD40 ligand and ICOS ligand prevents Foxp3$^+$ T cell depletion–triggered AMR. Our results suggested that activation of B cells depended on their interaction with T cells within the graft. We then analyzed expression levels of genes that are known to be important in the activation of B cells by Tfh cells. Expression levels of ICOS, ICOS ligand, CD40, and CD40 ligand, but not IL-21, were significantly elevated in Foxp3$^+$ T cell–depleted compared with control lung allografts (Figure 7A). We then treated recipients of Foxp3$^+$ T lymphocyte–depleted lung allografts with anti-ICOS ligand and anti-CD40 ligand. This regimen prevented graft rejection (Figure 7, B and C). We observed minimal peribronchial and perivascular collagen deposition (Figure 7D). The airway epithelium in these grafts appeared normal, with slightly elevated expression of CCSP and normal expression of AcT (Figure 7E). Furthermore, blocking ICOS ligand and CD40 ligand pathways inhibited the generation of DSA (Figure 7F).

Discussion

Our study took advantage of a lung retransplant model to conclusively demonstrate that graft-resident Foxp3$^+$ T cells maintain a tolerant state. Surprisingly, AMR following Foxp3$^+$ T lymphocyte depletion differs markedly from the cellular rejection pattern that we have previously reported in lungs following transplantation into nonimmunosuppressed hosts or when immunosuppression-mediated graft acceptance is abrogated by ischemia reperfusion injury or respiratory bacterial infection (10, 11). Our experiments indicate that depletion of Foxp3$^+$ T cells allows B and T cell interactions in lung allografts that result in the production of DSA and, ultimately, antibody-mediated destruction of the graft.

We have previously identified cell populations that are important for the induction of tolerance after lung transplantation. We showed that central memory CCR7$^+$CD62L^{hi}CD44^{hi} CD8$^+$ T cells induce acceptance of pulmonary allografts through IFN-γ–mediated production of nitric oxide (5). CCR7-mediated synapses between CD8$^+$ T cells and antigen-presenting cells within the lung allograft were important for the production of IFN-γ. More recently, we have demonstrated that graft-infiltrating eosinophils produce nitric oxide after stimulation with IFN-γ and that lungs are rejected when eosinophils are prevented from entering the graft (12). These findings demonstrate that immune events that regulate the induction of tolerance after pulmonary transplantation occur in the lung, setting this organ apart from other grafts in which downregulation of alloimmune responses depends on trafficking of cells to draining lymph nodes (4). We have now extended these observations to show that maintenance of immune tolerance after pulmonary transplantation is also regulated through cellular interactions in the graft. We demonstrate that hearts matching the strain of the original lung donor survive indefinitely without any evidence of graft rejection in the absence of additional immunosuppression. While third-party cardiac allografts are eventually rejected, they experience prolonged survival when transplanted into previous lung recipients. This observation is consistent with previous reports showing that, once activated, regulatory CD4$^+$ T cells can suppress immune responses in an antigen-nonspecific fashion (13). This phenomenon, which has been referred to as "bystander" regulation, has been demonstrated in vivo in the context of transplantation, where alloantigen-induced regulatory CD4$^+$ T cells are able to extend the survival of third-party skin allografts when reactivated by the original antigen (14). Of note, the existence of bystander regulation has raised concerns about the potential to compromise immunity to pathogens in transplant recipients, where tolerance is induced (15).

It has been the prevailing notion that the induction of tertiary lymphoid organs in allografts results in locally generated deleterious immune responses (16, 17). These structures have been observed in murine and human cardiac allografts that undergo either acute or chronic rejection (18, 19). Quilty lesions are endocardial lymphocytic infiltrates that have been observed in human heart grafts. To our knowledge, they lack hallmarks of organized tertiary lymphoid organs, such as PNAd-expressing high endothelial venules. While these lesions remain poorly understood, some studies have suggested that they are associated with adverse events due to immune-mediated graft injury (20, 21). In rat aortic allografts, B cells residing within tertiary lymphoid organs have been suggested as contributing to chronic rejection through the local production of alloantibodies (22). Similarly, induced BALT can propagate immune responses against viruses independently of secondary lymphoid organs (23). In contrast, we have previously reported that BALT is induced in long-term accepted lung allografts, which expresses peripheral node addressin — a hallmark of high endothelial venules — and is rich in Foxp3$^+$ T cells (7). Interestingly, BALT-bearing tolerant lungs survive after transplantation into nonimmunosuppressed hosts, suggesting that immunoregulatory pathways that are established within the graft protect the lung from immunological destruction. Using Foxp3-DTR mice as intermediate hosts in a retransplant model allowed us to conclusively show that graft-resident Foxp3$^+$ T lymphocytes, the vast majority of which form aggregates in the BALT, are critical to maintaining a tolerant state. The presence of regulatory T cells within transplanted tissues has been previously reported in murine skin grafts (24). Furthermore, there exist reports of Foxp3$^+$ T cell–rich organized lymphoid aggregates in spontaneously accepted murine kidney allografts (25). Interestingly, global depletion of Foxp3$^+$ T lymphocytes in recipient mice triggered cellular rejection of tolerant renal allografts, which was associated with graft infiltration by CD4$^+$ and CD8$^+$ T cells and an increased reactivity of recipient T cells against donor antigen. In contrast with our observations, depletion of Foxp3$^+$ T cells in renal allograft recipients did not result in changes in serum alloantibody levels, and grafts had no histological evidence of humoral rejection. Important differences exist between this study examining the role of Foxp3$^+$ T lymphocytes in maintaining tolerance of kidney allografts and our investigation in lung allograft tolerance. First, it has not been

explored whether immune responses that regulate the fate of kidney allografts occur in the graft itself or in draining secondary lymphoid organs. Unlike the BALT that is induced in tolerant lungs, Foxp3$^+$ T cell–rich nodular aggregates in tolerant renal grafts lack expression of peripheral node addressin. Therefore, trafficking patterns of immune cells may differ between tolerant lung and kidney grafts. Second, our retransplant model allowed us to target only Foxp3$^+$ T cells that reside in the tolerant graft, while global depletion of Foxp3$^+$ T lymphocytes in Foxp3-DTR recipients could lead to more widespread inflammatory responses.

AMR has been increasingly recognized as a cause of adverse outcomes in recipients of solid organ grafts (26, 27). Clinically, hallmarks of AMR of lungs include allograft dysfunction, presence of circulating DSA, capillary endothelial C4d deposition, and pathologic findings characteristic of acute lung injury, such as hyaline membrane formation (28). AMR cannot only lead to acute graft failure, but can also predispose patients to chronic lung allograft dysfunction (29). For example, a recent study identified de novo development of DSA as associated with an increased incidence of chronic allograft dysfunction after pulmonary transplantation (30). Similarly, obliterative bronchiolitis, a hallmark of chronic graft-versus-host disease following allogeneic bone marrow transplantation, was found to depend on production of alloantibodies by B cells in the donor inoculum (31). A recent study that employed transplantation of human arterial grafts into immunodeficient mice proposed a mechanistic link between humoral alloimmune responses and chronic rejection (32). The authors demonstrated that activation of endothelial cells through binding of alloantibodies and deposition of complement promoted the recruitment and activation of alloreactive T cells, which resulted in the development of chronic vasculopathy. In our study, we have observed that circulating DSA are associated with the development of airway lesions that resemble those present in human lungs that undergo chronic rejection. While we demonstrate an important role for recipient T cells in the activation of B lymphocytes, their production of DSA, and the promotion of AMR, it is possible that — following activation of graft cells by alloantibodies — alloreactive T lymphocyte populations contribute to or potentiate pathologic changes that are characteristic of chronic lung rejection. Mechanistically, several cell populations in lung allografts could be targets for antibody-mediated injury that results in airway remodeling. We found reduced expression of CCSP in lung grafts following depletion of Foxp3$^+$ T lymphocytes; this was similar to previous findings in human lungs that developed obliterative bronchiolitis (8). Club cells have been shown to play a role in tissue repair, and therefore, their loss may contribute to aberrant repair of injured airways in lung allografts (33). Alloantibody binding to ciliated airway epithelial cells in vitro can induce production of fibroblast growth factors, resulting in fibroblast proliferation (34). Endobronchial administration of antibodies directed against MHC class I or II molecules, which can target both ciliated and nonciliated airway epithelial cells, results in fibrotic airway changes that are reminiscent of those seen in human lung grafts that develop obliterative bronchiolitis (35, 36). We have observed complement deposition on the endothelium of small vessels after depletion of Foxp3$^+$ T cells. Interestingly, microvascular injury triggered by antibody-mediated complement activation results in graft ischemia in orthotopic tracheal transplants (37). There exists both clinical and experimental evidence that loss of microvessels and tissue ischemia are associated with and can lead to fibrotic airway remodeling (38, 39).

Currently, there exists no standardized, universally accepted treatment regimen for patients who suffer from AMR after lung transplantation. Therapeutic approaches have been adopted from larger experiences with the treatment of antibody-mediated diseases and generally include B cell depletion strategies, i.v. immunoglobulin, plasmapheresis, and proteasome inhibitors. It is well established that T cells need to provide help to B cells in order to generate antigen-specific antibody responses. Consistent with this notion, the presence of recipient T cells was required for the production of DSA following depletion of graft-resident Foxp3$^+$ T cells in our experiments. Antibody production following transplantation of allogeneic grafts has been shown to depend on interactions between CD4$^+$ T cells with indirect alloreactivity and MHC II molecules on B cells, and our intravital imaging demonstrates prolonged contact between recipient B and T cells in grafts that undergo AMR (40).

Tfh cells are specialized lymphocytes that express CXCR5 and high levels of PD-1 and ICOS, as well as the transcription factor Bcl-6, and can support antibody production by B cells through IL-21 as well as ICOS/ICOS ligand and CD40/CD40 ligand signaling. In addition, B cell help can be provided by other T cell populations. For example, IL-21–producing Tfh-like cells that lack expression of CXCR5 or Bcl6 have been described in inflamed tissues, where they can interact with B cells and promote their activation (41). While the frequencies of graft-infiltrating Tfh were not affected by depletion of graft-resident Foxp3$^+$ cells, our findings that inhibition of CXCL13 altered the behavior of graft-infiltrating CD4$^+$ T and B cells, as well as prevented the development of DSA and AMR, supports the notion that CXCR5-expressing T cells play an important role in triggering graft rejection in our model. Our findings extend recent observations in murine chronic graft-versus-host disease models in which development of fibrotic airway lesions could be prevented by similar interventions (42). Our imaging studies demonstrate that graft-resident Foxp3$^+$ T cells interact with both graft-infiltrating CD4$^+$ T and B cells and further suggest that DSA production and AMR following Foxp3$^+$ T cell depletion depend on encounters between CD4$^+$ T cells and B lymphocytes within the graft. Previous studies have shown that Foxp3$^+$ regulatory T cells can inhibit B cell responses. For example, global depletion of Foxp3$^+$ T lymphocytes in adult mice results in a CD4$^+$ T cell–dependent activation of B cells in secondary lymphoid organs and the production of autoantibodies (43). A population of Foxp3$^+$ T cells, referred to as Tfr cells, has been described that expresses markers characteristic of Tfh cells, including CXCR5, PD-1, and the transcription factor Bcl-6 (44). These Tfr cells can gain access to germinal centers, where they suppress B cell responses. Various mechanisms have been proposed as to how Foxp3$^+$ T cells can suppress humoral responses. They may prevent the expansion of Tfh cells, possibly through inhibiting the activation of dendritic cells (43). Also, Foxp3$^+$ T lymphocytes can directly inhibit Tfh cells or B lymphocytes, a process that has been shown to be dependent on their expression of CTLA4, which we have found to be expressed by the majority of graft-resident Foxp3$^+$ T cells (45, 46). In addition, Foxp3$^+$ T lymphocytes may prevent or disrupt interactions between Tfh cells and B lymphocytes. To this end, we have previously shown

that lymphocytes infiltrating tolerant lung allografts preferentially migrate to the induced BALT (7). Thus, our findings suggest that graft-infiltrating alloreactive B and T lymphocytes are inhibited following their encounter with Foxp3$^+$ T cells in the BALT, thereby preventing them from mounting alloimmune responses.

In conclusion, our observations advance our understanding of mechanisms that trigger AMR and have important implications for the clinical management of lung transplant patients. Our findings that BALT-resident Foxp3$^+$ T cells inhibit the generation of humoral responses substantiate the notion that local immune responses regulate the fate of transplanted lungs. Thus, strategies to induce and maintain Foxp3$^+$ T cell–rich BALT in pulmonary allografts may improve survival after lung transplantation. We suggest that the rapid tempo of AMR in our model is related to the pharmacologically induced rapid and complete depletion of graft-resident Foxp3$^+$ cells. Respiratory viral infections, an established risk factor for the generation of de novo DSA, have been shown to compromise the suppressive functions of pulmonary regulatory T cells (47). This raises the possibility that such infections can disrupt local immunoregulatory pathways in lung transplant patients and trigger AMR, albeit at a slower rate compared with the tempo observed in our model (47, 48). Given that AMR is largely refractory to current immunosuppression, our observations provide a rationale for targeting costimulatory or chemotactic pathways that promote the activation of B lymphocytes by Tfh cells.

Methods

Mice and reagents. B6 (CD45.2), B6.SJL-PtprcaPepcb/BoyJ (CD45.1), BALB/c, CBA/Ca, B6 Foxp3-DTR, B6 Foxp3 IRES-GFP, B6 nude, and B6.129S2-*Ighm^{tm1Cgn}*/J (muMt$^-$) mice were purchased from The Jackson Laboratory. B6 AID/μS KO mice were provided by G. Chalassani (University of Pittsburgh, Pittsburgh, Pennsylvania, USA) after obtaining permission from F. Lund (University of Alabama, Birmingham, Alabama, USA) (9). Primary lung transplant recipients were treated with costimulatory blockade consisting of anti-CD40 ligand (250 μg i.p.) and CTLA4-Ig (200 μg i.p.) on days 0 and 2, respectively (Bio X Cell). To deplete graft-resident Foxp3$^+$ cells, DT (List Biologic Laboratories Inc.) (1 μg i.p.) was administered at the time of retransplantation (days 0, 1) to secondary recipients receiving grafts that had initially been transplanted into Foxp3-DTR hosts. Some retransplant recipients were treated with anti-ICOS ligand (200 μg i.p., days 0, 2, 4, 6) and anti-CD40 ligand antibodies (250 μg i.p., days 0, 2, 4, 6) or anti-murine CXCL13 antibodies (200 μg i.p., days 0, 2, 4, 6, after retransplantation for survival studies; and 200 μg i.p., days 0, 1, 2, for intravital imaging studies) (R&D Systems). Six- to ten-week-old mice were used for the studies. Sex-matched mice were used for the transplant procedures.

Surgical procedures. Orthotopic murine left lung transplants and retransplants as well as heterotopic heart transplants into the recipient's right neck were performed as previously described (49–51).

Flow cytometry. Lung tissue was digested, and single-cell suspensions were prepared as previously described (5, 49). Cells were then stained using CD45.2 (clone 104; Thermofisher), CD45.1 (clone A20; BD Biosciences), CD90.2 (clone 53-2.1; Thermofisher), CD4 (clone RM4-5; Biolegend), CD8α (clone 53.6.7; Thermofisher), CD62L (clone MEL-14; Biolegend), CD44 (clone IM7; eBiosciences), CD25 (clone PC61; Biolegend), Fas (clone Jo2; BD Biosciences), GL7 (clone GL7; BD Biosciences), B220 (clone RA3-6B2; eBiosciences), CD19 (clone 1D3; BD Biosciences), CXCR5 (clone 2G8; BD Biosciences), PD-1 (clone J43; Thermofisher), Foxp3 (clone FJK-16s; Thermofisher), CTLA4 (clone UC10-4F10-11; BD Biosciences), perforin (clone eBio-OMAK-D; Thermofisher), granzyme B (clone NGZB; Thermofisher), Ki-67 (clone SolA15; Thermofisher), Bcl-6 (clone K112-g1; BD Biosciences), and isotype control antibodies (BD Biosciences, BioLegend, eBioscience, R&D Systems). Intracellular staining (Foxp3, CTLA4, Ki-67, Bcl-6, perforin, granzyme B) was performed as previously described (5). For determination of serum alloantibody titers, 200 μl aliquots of PBS with 0.5% BSA and 0.02% sodium azide (PBA) containing 2×10^6 BALB/c, B6, or CBA/Ca thymocytes were mixed with 200 μl of serially diluted serum for 1 hour at 4°C with frequent agitation. After 3 washes with PBA, cells were stained for 30 minutes at 4°C with 100 μl of PBA containing 1 μl of polyclonal fluorochrome-conjugated goat anti-mouse IgM (μ chain specific) or anti-mouse IgG (Fcγ fragment specific) (Jackson ImmunoResearch). Cells were analyzed on a FACScan (BD Biosciences), and FlowJo software (FlowJo) was used to calculate the median fluorescence intensity.

Two-photon microscopy. Lung grafts were imaged by intravital 2-photon microscopy at indicated time points for periods of up to 3 hours, as previously described (52). Quantum dots (655 nm, 30 μl) (Life Technologies) were injected to label vessels. CD4$^+$ T and B cells were isolated via positive selection with CD4 and B220 magnetic beads, respectively, from spleens of B6 mice (Miltenyi Biotec). We injected 2×10^7 CD4$^+$ T cells and 2×10^7 B cells, labeled with CFSE, CMTMR, or CellTrace Violet, as indicated for respective experiments, into lung recipients 24 hours prior to imaging (Life Technologies). Grafts were exposed and imaged with a custom 2-photon microscope using ImageWarp (A&B Software). Sequential z-sections (2.5 μm each) were acquired, yielding an imaging volume of $220 \times 247.5 \times 50$ μm^3. Analyses were performed with Imaris (Bitplane). For each mouse, up to 5 lung areas at least 80 μm deep were analyzed (5).

Quantitative PCR. Homogenized lung graft tissue was lysed with TRIzol (Thermo Fisher Scientific), as previously described (53). Total RNA was isolated using QIAGEN RNeasy Mini Kit (QIAGEN), and quantitative PCR was performed as previously described. Primer sequences were as follows: ICOS, 5′-ATGAAGCCGTACTTCTGCCG-3′ and 5′-CGCATTTTTAACTGCTGGACAG-3′; ICOSL, 5′-TAAAGTGTCCCTGTTTTGTGTCC-3′ and 5′-ATTGCACCGACTTCAGTCTCT-3′; CD40L, 5′-CCTTGCTGAACTGTGAGGAGA-3′ and 5′-CTTCGCTTACAACGTGTGCT-3′; CD40, 5′-TGTCATCTGTGAAAAGGTGGTC-3′ and 5′-ACTGGAGCAGCGGTGTTATG-3′; and IL-21, 5′-TGCATCAGTGACGGTAAACCA-3′ and 5′-CACAGTTTGGAGTGTTGAGGAT-3′.

Histology. Transplanted mouse lungs or hearts as well as human transbronchial biopsies were fixed in formaldehyde, sectioned, and stained with H&E (lungs and hearts) or MT (lungs). A surgical pathologist blinded to the experimental conditions assessed grafts stained with H&E for rejection.

Immunostaining. For immunohistochemistry, formalin-fixed, 5 μm sections of paraffin-embedded specimens were deparaffinized and rehydrated. Following antigen retrieval in citrate buffer (pH 6.0, Dako), endogenous peroxide activity was quenched with 3% H_2O_2. The slides were washed in PBS with 1.5% BSA and 0.1% Tween-20 (PBT). Nonspecific immunobinding sites were blocked with 10% normal rabbit serum (Vector S-5000) or serum-free protein block (Dako) for PNAd or Foxp3/CXCL13, respectively. For Foxp3 and CXCL13 staining, the specimens were sequentially incubated in avidin D and biotin blocking solution

(Vector Laboratories). Sections were incubated with primary antibodies overnight at 4°C in a humidified chamber. Primary antibodies used were rabbit monoclonal anti-human Foxp3 (clone SP97, 1:400, Novus), rabbit polyclonal anti-mouse CXCL13 (1:100, Bioss), and rat monoclonal anti-mouse PNAd (clone MECA-79, 1:100, BD Biosciences). Following primary antibody labeling, slides were washed in PBT and then incubated with biotin-conjugated goat anti-rabbit (Foxp3 and CXCL13) or anti-rat (PNAd) IgG for 30 minutes. Antibody-binding sites were amplified using Vectastain ABC kit and visualized with 3,3-diaminobenzidine as a peroxidase substrate (Vector Laboratories). After counterstaining with Gill's hematoxylin and washing in water, sections were dehydrated and mounted. Staining for C4d was performed as previously described (54).

Fluorescent immunostaining was performed for B220 and CD3. Following deparaffinization, antigen retrieval was performed (Diva Decloaker, Biocare) and specimens were washed with tris-buffered saline and Tween-20 (TBST). Nonspecific immunobinding sites were blocked with 10% normal rabbit serum (Vector S-5000). Sections were incubated with either rabbit anti-mouse CD3 (clone SP7, 1:100, Abcam) or rat anti-mouse B220/CD45R (clone RA3-6B2, 1:200, BD Biosciences) primary antibodies overnight at 4°C in a humidified chamber. Specimens were again washed with TBST and incubated with the secondary antibody goat anti-rabbit Alexa Fluor 568 (1:200, Abcam) or goat anti-rat Alexa Fluor 488 (1:200, Abcam) for CD3 and B220 staining, respectively. Specimens were then washed in TBST, incubated overnight with IB4 Alexa Fluor 647 (1:1000, Thermo Fisher. Scientific), washed, and then incubated for 30 minutes with Hoechst 33342 (1:1000, Thermo Fisher. Scientific).

Airway staining. Formalin-fixed, 5 μm sections of paraffin-embedded specimens were deparaffinized and washed in PBS. Following antigen retrieval in citrate buffer (pH 6.0), slides were blocked (5% BSA, 1× PBS). Subsequently, sections were incubated with primary antibodies overnight at 4°C in a humidified chamber. The primary antibodies used were rabbit polyclonal anti-rat CCSP (1:500, Abcam) and mouse IgG2b anti-AcT (1:12,000, MilliporeSigma). Following primary antibody labeling, slides were washed in PBS and then incubated with Alexa Fluor 594 donkey anti-rabbit IgG and Alexa Fluor 488 goat anti-mouse IgG2b (1:500, Invitrogen) for 90 minutes at room temperature. Slides were extensively washed in PBS and coverslipped with DAPI (MilliporeSigma) in Fluoromount-G mounting media (Southern Biotech). Images were obtained using a Zeiss Observer.Z1 inverted fluorescent microscope (Carl Zeiss Inc.) equipped with a digital camera and processed using AxioVision release 4.6.3 (Carl Zeiss) software.

Statistics. Data were analyzed with the Mann-Whitney *U* test, which was performed using GraphPad Prism, version 7.0 (GraphPad Software). Data were graphed as mean ± SEM. Cardiac allograft survival was compared between groups with Kaplan-Meier analysis. Data were considered statistically significant at $P < 0.05$.

Study approval. Animal experiments were approved by the Institutional Animal Studies Committee at Washington University. Animals received humane care in compliance with the *Guide for the Care and Use of Laboratory Animals* (National Academies Press, 2011) and with the Principles of Laboratory Animal Care formulated by the National Society for Medical Research. Human protocols were approved by the Institutional Review Board at Washington University School of Medicine (no. 201811073). Patients provided informed consent.

Author contributions

WL, JMG, RH, HMH, ST, LV, WMB, FLK, BWW, and AYT conducted experiments. WL, JHR, RRH, VP, AB, ASK, CSH, WMB, SMP, and AEG contributed to study design and reviewed and revised the manuscript. WL, JMG, RH, and DK analyzed and interpreted the data. WL, JMG, and DK wrote the manuscript. DK designed and supervised the study.

Acknowledgments

This work was supported by NIH grants 1P01AI116501, R01 HL094601, and 1F32HL-143950, Veterans Administration Merit Review grant 1I01BX002730, and the Foundation for Barnes-Jewish Hospital.

Address correspondence to: Daniel Kreisel, Pathology and Immunology, Campus Box 8234, 660 South Euclid Avenue, Washington University School of Medicine, St. Louis, Missouri 63110, USA. Phone: 314.362.6021; Email: kreiseld@wustl.edu.

1. Chambers DC, et al. The Registry of the International Society for Heart and Lung Transplantation: Thirty-fourth Adult Lung And Heart-Lung Transplantation Report-2017; Focus Theme: Allograft ischemic time. *J Heart Lung Transplant*. 2017;36(10):1047–1059.
2. Witt CA, Puri V, Gelman AE, Krupnick AS, Kreisel D. Lung transplant immunosuppression - time for a new approach? *Expert Rev Clin Immunol*. 2014;10(11):1419–1421.
3. Lakkis FG, Arakelov A, Konieczny BT, Inoue Y. Immunologic 'ignorance' of vascularized organ transplants in the absence of secondary lymphoid tissue. *Nat Med*. 2000;6(6):686–688.
4. Zhang N, et al. Regulatory T cells sequentially migrate from inflamed tissues to draining lymph nodes to suppress the alloimmune response. *Immunity*. 2009;30(3):458–469.
5. Krupnick AS, et al. Central memory CD8+ T lymphocytes mediate lung allograft acceptance. *J Clin Invest*. 2014;124(3):1130–1143.
6. Gelman AE, et al. Cutting edge: Acute lung allograft rejection is independent of secondary lymphoid organs. *J Immunol*. 2009;182(7):3969–3973.
7. Li W, et al. Lung transplant acceptance is facilitated by early events in the graft and is associated with lymphoid neogenesis. *Mucosal Immunol*. 2012;5(5):544–554.
8. Kelly FL, et al. Epithelial clara cell injury occurs in bronchiolitis obliterans syndrome after human lung transplantation. *Am J Transplant*. 2012;12(11):3076–3084.
9. Zeng Q, et al. B cells mediate chronic allograft rejection independently of antibody production. *J Clin Invest*. 2014;124(3):1052–1056.
10. Kreisel D, et al. Emergency granulopoiesis promotes neutrophil-dendritic cell encounters that prevent mouse lung allograft acceptance. *Blood*. 2011;118(23):6172–6182.
11. Yamamoto S, et al. Cutting edge: Pseudomonas aeruginosa abolishes established lung transplant tolerance by stimulating B7 expression on neutrophils. *J Immunol*. 2012;189(9):4221–4225.
12. Onyema OO, et al. Eosinophils promote inducible NOS-mediated lung allograft acceptance. *JCI Insight*. 2017;2(24):e96455.
13. Thornton AM, Shevach EM. Suppressor effector function of CD4+CD25+ immunoregulatory T cells is antigen nonspecific. *J Immunol*. 2000;164(1):183–190.
14. Karim M, Feng G, Wood KJ, Bushell AR. CD25+CD4+ regulatory T cells generated by exposure to a model protein antigen prevent allograft rejection: antigen-specific reactivation in vivo is critical for bystander regulation. *Blood*. 2005;105(12):4871–4877.
15. Zhao Y, Li X. Cross-immune tolerance: conception and its potential significance on transplantation tolerance. *Cell Mol Immunol*. 2010;7(1):20–25.
16. Hsiao HM, Li W, Gelman AE, Krupnick AS, Kreisel D. The role of lymphoid neogenesis in allografts. *Am J Transplant*. 2016;16(4):1079–1085.
17. Thaunat O, Patey N, Morelon E, Michel JB, Nicoletti A. Lymphoid neogenesis in chronic rejection: the murderer is in the house. *Curr Opin*

Immunol. 2006;18(5):576–579.
18. Baddoura FK, Nasr IW, Wrobel B, Li Q, Ruddle NH, Lakkis FG. Lymphoid neogenesis in murine cardiac allografts undergoing chronic rejection. *Am J Transplant*. 2005;5(3):510–516.
19. Huibers MM, et al. The composition of ectopic lymphoid structures suggests involvement of a local immune response in cardiac allograft vasculopathy. *J Heart Lung Transplant*. 2015;34(5):734–745.
20. Hiemann NE, Knosalla C, Wellnhofer E, Lehmkuhl HB, Hetzer R, Meyer R. Quilty in biopsy is associated with poor prognosis after heart transplantation. *Transpl Immunol*. 2008; 19(3–4):209–214.
21. Smith RN, Chang Y, Houser S, Dec GW, Grazette L. Higher frequency of high-grade rejections in cardiac allograft patients after Quilty B lesions or grade 2/4 rejections. *Transplantation*. 2002;73(12):1928–1932.
22. Thaunat O, et al. Lymphoid neogenesis in chronic rejection: evidence for a local humoral alloimmune response. *Proc Natl Acad Sci U S A*. 2005;102(41):14723–14728.
23. Moyron-Quiroz JE, et al. Role of inducible bronchus associated lymphoid tissue (iBALT) in respiratory immunity. *Nat Med*. 2004;10(9):927–934.
24. Graca L, Cobbold SP, Waldmann H. Identification of regulatory T cells in tolerated allografts. *J Exp Med*. 2002;195(12):1641–1646.
25. Miyajima M, et al. Early acceptance of renal allografts in mice is dependent on foxp3(+) cells. *Am J Pathol*. 2011;178(4):1635–1645.
26. Wan SS, Ying TD, Wyburn K, Roberts DM, Wyld M, Chadban SJ. The treatment of antibody-mediated rejection in kidney transplantation: an updated systematic review and meta-analysis. *Transplantation*. 2018;102(4):557–568.
27. Colvin MM, et al. Antibody-mediated rejection in cardiac transplantation: emerging knowledge in diagnosis and management: a scientific statement from the American Heart Association. *Circulation*. 2015;131(18):1608–1639.
28. Witt CA, et al. Acute antibody-mediated rejection after lung transplantation. *J Heart Lung Transplant*. 2013;32(10):1034–1040.
29. Aguilar PR, et al. The role of C4d deposition in the diagnosis of antibody-mediated rejection after lung transplantation. *Am J Transplant*. 2018;18(4):936–944.
30. Tikkanen JM, et al. De novo DQ donor-specific antibodies are associated with chronic lung allograft dysfunction after lung transplantation. *Am J Respir Crit Care Med*. 2016;194(5):596–606.
31. Srinivasan M, et al. Donor B-cell alloantibody deposition and germinal center formation are required for the development of murine chronic GVHD and bronchiolitis obliterans. *Blood*. 2012;119(6):1570–1580.
32. Jane-Wit D, et al. Alloantibody and complement promote T cell-mediated cardiac allograft vasculopathy through noncanonical nuclear factor-κB signaling in endothelial cells. *Circulation*. 2013;128(23):2504–2516.
33. Giangreco A, Arwert EN, Rosewell IR, Snyder J, Watt FM, Stripp BR. Stem cells are dispensable for lung homeostasis but restore airways after injury. *Proc Natl Acad Sci U S A*. 2009;106(23):9286–9291.
34. Jaramillo A, Smith CR, Maruyama T, Zhang L, Patterson GA, Mohanakumar T. Anti-HLA class I antibody binding to airway epithelial cells induces production of fibrogenic growth factors and apoptotic cell death: a possible mechanism for bronchiolitis obliterans syndrome. *Hum Immunol*. 2003;64(5):521–529.
35. Fukami N, et al. Antibodies to MHC class I induce autoimmunity: role in the pathogenesis of chronic rejection. *J Immunol*. 2009;182(1):309–318.
36. Takenaka M, Tiriveedhi V, Subramanian V, Hoshinaga K, Patterson AG, Mohanakumar T. Antibodies to MHC class II molecules induce autoimmunity: critical role for macrophages in the immunopathogenesis of obliterative airway disease. *PLoS ONE*. 2012;7(8):e42370.
37. Khan MA, et al. CD4+ T cells and complement independently mediate graft ischemia in the rejection of mouse orthotopic tracheal transplants. *Circ Res*. 2011;109(11):1290–1301.
38. Babu AN, et al. Microvascular destruction identifies murine allografts that cannot be rescued from airway fibrosis. *J Clin Invest*. 2007;117(12):3774–3785.
39. Luckraz H, et al. Microvascular changes in small airways predispose to obliterative bronchiolitis after lung transplantation. *J Heart Lung Transplant*. 2004;23(5):527–531.
40. Conlon TM, et al. Germinal center alloantibody responses are mediated exclusively by indirect-pathway CD4 T follicular helper cells. *J Immunol*. 2012;188(6):2643–2652.
41. Vu Van D, et al. Local T/B cooperation in inflamed tissues is supported by T follicular helper-like cells. *Nat Commun*. 2016;7:10875.
42. Flynn R, et al. Increased T follicular helper cells and germinal center B cells are required for cGVHD and bronchiolitis obliterans. *Blood*. 2014;123(25):3988–3998.
43. Leonardo SM, De Santis JL, Gehrand A, Malherbe LP, Gauld SB. Expansion of follicular helper T cells in the absence of Treg cells: implications for loss of B-cell anergy. *Eur J Immunol*. 2012;42(10):2597–2607.
44. Linterman MA, et al. Foxp3+ follicular regulatory T cells control the germinal center response. *Nat Med*. 2011;17(8):975–982.
45. Sage PT, Paterson AM, Lovitch SB, Sharpe AH. The coinhibitory receptor CTLA-4 controls B cell responses by modulating T follicular helper, T follicular regulatory, and T regulatory cells. *Immunity*. 2014;41(6):1026–1039.
46. Wing JB, Ise W, Kurosaki T, Sakaguchi S. Regulatory T cells control antigen-specific expansion of Tfh cell number and humoral immune responses via the coreceptor CTLA-4. *Immunity*. 2014;41(6):1013–1025.
47. Krishnamoorthy N, et al. Early infection with respiratory syncytial virus impairs regulatory T cell function and increases susceptibility to allergic asthma. *Nat Med*. 2012;18(10):1525–1530.
48. Kulkarni HS, Bemiss BC, Hachem RR. Antibody-mediated rejection in lung transplantation. *Curr Transplant Rep*. 2015;2(4):316–323.
49. Okazaki M, et al. A mouse model of orthotopic vascularized aerated lung transplantation. *Am J Transplant*. 2007;7(6):1672–1679.
50. Li W, et al. Intravital 2-photon imaging of leukocyte trafficking in beating heart. *J Clin Invest*. 2012;122(7):2499–2508.
51. Li W, et al. Surgical technique for lung retransplantation in the mouse. *J Thorac Dis*. 2013;5(3):321–325.
52. Kreisel D, et al. In vivo two-photon imaging reveals monocyte-dependent neutrophil extravasation during pulmonary inflammation. *Proc Natl Acad Sci U S A*. 2010;107(42):18073–18078.
53. Spahn JH, et al. DAP12 expression in lung macrophages mediates ischemia/reperfusion injury by promoting neutrophil extravasation. *J Immunol*. 2015;194(8):4039–4048.
54. Murata K, et al. Synergistic deposition of C4d by complement-activating and non-activating antibodies in cardiac transplants. *Am J Transplant*. 2007;7(11):2605–2614.